EFFECTS OF STRAIN AND SPIN–ORBIT COUPLING ON THE ELECTRONIC AND OPTICAL PROPERTIES OF MOS_2 AND $MOSE_2$ MONOLAYERS

Dao Minh Duc[1], Assoc.Prof., Dr. Le Tien Ha[1], Assoc.Prof., Dr. Tran Quang Huy[2], Dr. Luong Thi Theu[3]
[1]Thai Nguyen University of Sciences, Thai Nguyen University
[2]Faculty of Physics, Hanoi Pedagogical University 2
[3]Faculty of Economics and Fundamental Sciences, Hoa Binh University
Corresponding author: lttheu@daihochoabinh.edu.vn

Ngày nhận: 01/04/2026
Ngày nhận bản sửa: 03/4/2026
Ngày duyệt đăng: 24/4/2026
DOI: 10.71192/670136iwqkls

Abstract

This study systematically investigatesthe electronic and optical properties of monolayer MoX_2 (X = S, Se) under the combined effects of uniaxial strain and spin–orbit coupling (SOC) using density functional theory (DFT). The calculated band structures reveal that both MoS_2 and $MoSe_2$ exhibit direct band gaps at the K point, with values of approximately 1.78 eV and 1.44 eV, respectively. A significant SOC-induced splitting of the valence band maximum is observed, leading to the formation of two distinct excitonic transitions, namely A and B excitons. The energy separation between these excitons is found to be 0.15 eV for MoS_2 and 0.22 eV for $MoSe_2$. The influence of uniaxial strain is analyzed in the range of -5% to +5%, revealing that tensile strain reduces the band gap, whereas compressive strain slightly increases it. Notably, $MoSe_2$ exhibits a stronger sensitivity to strain compared to MoS_2. In addition, strain modifies the relative positions of band extrema and may induce a direct-to-indirect band gap transition under compressive conditions. Optical absorption spectra indicate strong excitonic peaks in the visible region, with clear strain-dependent shifts. MoS_2 exhibits higher exciton binding energy and sharper optical features, whereas $MoSe_2$ shows enhanced SOC effects and larger excitonic splitting. These findings highlight the critical interplay between strain and SOC in tuning the optoelectronic properties of two-dimensional transition metal dichalcogenides, providing valuable insights for the design of next-generation nanoscale optoelectronic and spintronic devices.

Keywords: *MoS_2 and $MoSe_2$ monolayers; Transition-metal dichalcogenides; Density functional theory; SOC; Excitons; Band structure; Density of states.*

Ảnh hưởng của biến dạng và tương tác spin-quỹ đạo lên tính chất điện tử và quang học của các lớp đơn MoS_2 và $MoSe_2$

SV. Đào Minh Đức[1], PGS.TS. Lê Tiến Hà[1], PGS.TS. Trần Quang Huy[2], TS. Lương Thị Thêu[3]
[1]Trường Đại học Khoa học, Đại học Thái Nguyên
[2]Khoa Vật lý, Trường Đại học Sư phạm Hà Nội 2
[3]Khoa Kinh tế và Khoa học cơ bản, Trường Đại học Hòa Bình
Tác giả liên hệ: lttheu@daihochoabinh.edu.vn.

Tóm tắt

Nghiên cứu này trình bày một khảo sát có hệ thống về các tính chất điện tử và quang học của đơn lớp MoX_2 (X = S, Se) dưới tác động kết hợp của biến dạng đơn trục và tương tác spin-quỹ đạo (SOC), sử dụng phương pháp lý thuyết phiếm hàm mật độ (DFT). Kết quả cho thấy cả MoS_2 và $MoSe_2$ đều có vùng cấm trực tiếp tại điểm K, với giá trị lần lượt khoảng 1,78 eV và 1,44 eV. Sự tách mức đáng kể của đỉnh vùng hóa trị do SOC gây ra dẫn đến sự hình thành hai chuyển tiếp exciton đặc trưng A và B, với độ chênh lệch năng lượng lần lượt khoảng 0,15 eV và 0,22 eV. Ảnh hưởng của biến dạng đơn trục được phân tích trong khoảng từ -5% đến +5%, cho thấy biến dạng kéo làm giảm độ rộng vùng cấm, trong khi biến dạng nén làm tăng nhẹ giá trị này. Đáng chú ý, $MoSe_2$ thể hiện độ nhạy với biến dạng lớn hơn so với MoS_2. Ngoài ra, biến dạng còn làm thay đổi vị trí các cực trị vùng năng lượng và có thể gây ra chuyển pha từ vùng cấm trực tiếp sang gián tiếp dưới điều kiện nén. Phổ hấp thụ quang học cho thấy các đỉnh exciton rõ rệt trong vùng khả kiến với sự dịch chuyển phụ thuộc vào biến dạng. MoS_2 đặc trưng bởi năng lượng liên kết exciton lớn hơn và các đỉnh quang học sắc nét hơn, trong khi $MoSe_2$ biểu hiện hiệu ứng SOC mạnh hơn cùng với độ tách exciton lớn hơn. Những kết quả này làm nổi bật vai trò tương tác giữa biến dạng và SOC trong việc điều chỉnh các tính chất quang-điện tử của vật liệu hai chiều, qua đó cung cấp cơ sở khoa học quan trọng cho việc thiết kế các thiết bị quang điện tử và spintronics thế hệ mới.

Từ khóa: *MoS_2 và $MoSe_2$ đơn lớp; Chalcogenide kim loại chuyển tiếp; lý thuyết hàm mật độ; tương tác spin-orbit; Exciton; cấu trúc dải năng lượng; mật độ trạng thái.*

1. Introduction

In recent years, two-dimensional (2D) materials have attracted tremendous research interest owing to their unique physical properties and promising applications in next-generation electronic and optoelectronic devices [1], [2]. Among these materials, transition metal dichalcogenides (TMDCs), such as MoS_2 and $MoSe_2$, have emerged as particularly important systems due to their intrinsic semiconducting nature and sizable band gaps [3-4]. Unlike graphene, which is gapless, monolayer TMDCs exhibit a direct band gap located at the K point of the Brillouin zone, enabling efficient light–matter interaction and making them highly suitable for applications in photodetectors, light-emitting devices, and solar energy conversion [1], [5].

One of the most remarkable features of monolayer TMDCs is the strong manifestation of exciton effects. Due to reduced dimensionality and weak dielectric screening, the Coulomb interaction between electrons and holes is significantly enhanced, leading to large exciton binding energies and stable excitonic states even at room temperature [6-8]. These excitonic effects give rise to distinct optical signatures, typically observed as A and B exciton peaks in absorption and photoluminescence spectra [6], [8]. The energy separation between these peaks is closely related to the splitting of the valence band, which is primarily governed by SOC [9-10]. SOC plays a crucial role in determining the fine structure of the electronic band structure. In TMDCs, SOC induces a significant splitting of the valence band maximum at the K point, resulting in two spin-polarized sub-bands [9-10]. This splitting directly influences the optical transition energies and the relative positions of A and B excitons [11]. Moreover, the strength of SOC depends strongly on the atomic number of the chalcogen element; therefore, $MoSe_2$ exhibits a larger valence band splitting compared to MoS_2 [10-11]. This difference leads to observable variations in their optical spectra and excitonic behavior, highlighting the importance of relativistic effects in these materials.

In addition to their intrinsic properties, the electronic and optical characteristics of TMDCs can be effectively tuned by external perturbations, among which mechanical strain has proven to be one of the most versatile approaches [12-13]. Strain engineering can modify interatomic distances and orbital hybridization, thereby altering the band structure, band gap magnitude, and even the nature of the band gap [12], [14]. In particular, strain can induce a transition from a direct to an indirect band gap, significantly affecting the optical efficiency of the material [2], [14]. When combined with SOC, strain introduces a complicated interaction between lattice deformation and spin–orbit interactions, leading to nontrivial modifications in both electronic and optical responses [14-15]. Understanding the combined effects of strain and SOC is therefore essential for tailoring the optoelectronic properties of TMDCs for practical applications. In this regard, DFT has become a powerful and widely used theoretical framework for investigating material properties at the atomic level [16-17]. DFT allows for accurate calculations of band structures, density of states, and optical properties, providing valuable insights into the underlying physical mechanisms [18-19].

In this work, we perform a systematic first-principles study of the effects of both compressive and tensile strain on the electronic and optical properties of monolayer MoS_2 and $MoSe_2$, explicitly including SOC in the calculations. By analyzing the evolution of band structures, density of states, and excitonic features under strain, we aim to elucidate the fundamental mechanisms governing strain-induced modifications. The results of this study not only deepen the understanding of the interplay between strain and relativistic effects in 2D materials but also provide useful guidelines for the design and optimization of high-performance optoelectronic devices based on TMDCs.

2. Computational Methods

All first-principles calculations were performed within the framework of DFT as implemented in the *Vienna Ab initio Simulation Package* (VASP) [18], [20]. The interaction between ion cores and valence electrons was described using the projector augmented-wave (PAW) method [19], [21]. A plane-wave basis set with a kinetic energy cutoff of 500 eV was employed to ensure numerical accuracy. To eliminate spurious interactions between periodically repeated layers, a vacuum spacing of approximately 15 Å was introduced along the out-of-plane direction, preserving the intrinsic two-dimensional nature of the systems.

A series of exchange–correlation functionals, including the generalized gradient approximation (GGA) [22], vdW-DF2 [23], optPBE-vdW, optB88-vdW, optB86b-vdW, and revPBE-vdW [24], were systematically evaluated to determine the most suitable functional for describing the structural properties of the materials. Among these, the optPBE-vdW functional was found to yield lattice parameters in closest agreement with experimental data for both MoS_2 and $MoSe_2$, and was therefore adopted in all subsequent calculations. The Brillouin zone was sampled using a Monkhorst–Pack k-point mesh of 25×25×1 [25]. The convergence criterion for the total energy was set to 10^{-5} eV, and all atomic positions were fully relaxed until

the residual forces on each atom were less than 0.01 eV/Å. The lattice constants were optimized prior to electronic structure calculations.

Spin–orbit coupling was explicitly included in all electronic structure calculations, as it plays a crucial role in transition metal dichalcogenides containing heavy elements [9], [26]. In particular, SOC induces a pronounced spin splitting of the valence band maximum at high-symmetry points such as K and Q in the Brillouin zone, which is essential for accurately describing excitonic transitions.

Uniaxial strain was applied by uniformly modifying the in-plane lattice constant according to the relation:

$$\varepsilon = \frac{a - a_0}{a_0} \times 100\%$$

where a_0 and a denote the equilibrium and strained lattice constants, respectively. Both tensile ($\varepsilon > 0$) and compressive ($\varepsilon < 0$) strains were considered within the range of −5% to +5%, consistent with the mechanically accessible limits reported for two-dimensional materials [27]. After applying strain, the atomic positions were fully relaxed while keeping the in-plane lattice parameters fixed, ensuring that the system reached a new equilibrium configuration under the imposed deformation.

Finally, the electronic band structures were calculated along the high-symmetry path M–Γ–K–M in the Brillouin zone, enabling a comprehensive characterization of the key electronic features, including band gap evolution, valley shifts, and SOC-induced band splitting.

The optical response was evaluated in terms of the complex dielectric function, where the imaginary component captures the interband transition processes and the real component is obtained through the Kramers–Kronig transformation. These calculations were carried out in a non-self-consistent manner using the LOPTICS implementation within VASP [28].

3. Results and Discussion

3.1. Electronic Structure and SOC-Induced Band Splitting

The electronic band structures of monolayer MoS_2 and $MoSe_2$, including SOC, are shown in Figure 3.1.

Figure 3.1. Band structures of MoS_2 and $MoSe_2$ with SOC

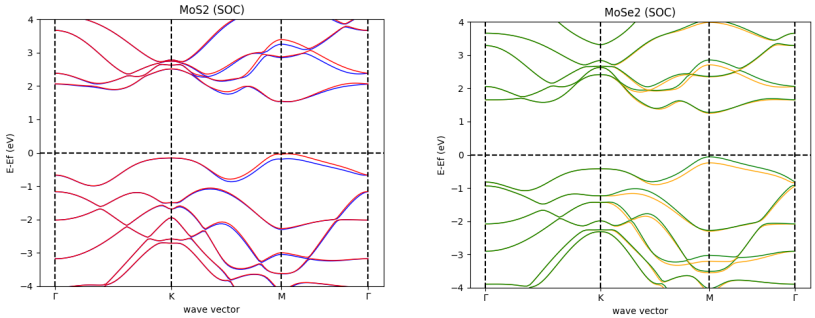

Both materials exhibit a direct band gap at the K point, which is a defining feature for efficient light absorption and emission in TMDCs. The calculated band gaps are approximately 1.78 eV for MoS_2 and 1.44 eV for $MoSe_2$, indicating that $MoSe_2$ possesses a narrower band gap due to the weaker electronegativity and larger atomic size of Se compared to S. A prominent feature observed in both systems is the spin–orbit coupling-induced splitting of the valence band maximum (VBM) at the K point. The splitting is calculated to be approximately 0.15 eV for MoS_2 and 0.22 eV for $MoSe_2$, demonstrating a stronger SOC effect in $MoSe_2$. This behavior originates from the heavier atomic mass of Se, which enhances relativistic interactions. Meanwhile, the conduction band minimum (CBM) remains nearly spin-degenerate due to its dominant Mo-*d* orbital character.

3.2. Excitonic Transitions and Their Physical Origin

The SOC-induced valence band splitting gives rise to two distinct excitonic transitions, known as A and B excitons, as illustrated in Figure 3.2.

Figure 3.2. Schematic diagram of A and B excitons at K point

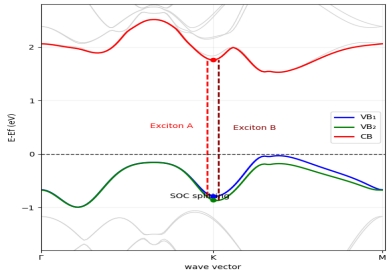

The A exciton corresponds to the transition from the VB_1 to the CBM, while the B exciton originates from the lower spin-split valence band ($VB_2 \rightarrow$ CBM). These transitions dominate the optical spectra of TMDC monolayers. The extracted excitonic transition energies are summarized in Table 3.1.

Table 3.1. Electronic and excitonic properties of monolayer MoS_2 and $MoSe_2$ (including SOC)

Material	Band gap (eV)	VBM splitting (eV)	A exciton (eV)	B exciton (eV)	ΔE (eV)	Exciton binding energy (eV)
MoS_2	1.78	0.15	1.78	1.93	0.15	0.45 – 0.55
$MoSe_2$	1.44	0.22	1.44	1.66	0.22	0.30 – 0.40

As shown in Table 3.1, the energy separation between A and B excitons (ΔE) matches closely with the SOC-induced VBM splitting, confirming the physical origin of these optical transitions. Furthermore, MoS_2 exhibits a larger exciton binding energy compared to $MoSe_2$, indicating stronger Coulomb interaction and weaker dielectric screening.

3.3. Strain-Induced Band Gap Engineering

To investigate the tunability of electronic properties, biaxial strain ranging from −5% to +5% was applied. The variation of band gap under strain is presented in Table 3.2.

Table 3.2. Strain-dependent electronic structure and excitonic parameters of monolayer MoS_2 and $MoSe_2$. The band gap type (direct/indirect), spin–orbit splitting at the valence band maximum (ΔSO), exciton binding energy (E), and ΔA–B excitonic transition energies are summarized under compressive (−5%) and tensile (+5%) strain conditions.

Material	Strain	Band gap (eV)	Gap type	ΔSO (VBM) (eV)	Eb exciton (eV)	A-exciton (eV)	B-exciton (eV)	ΔA–B (eV)
MoS_2	−5%	1.30	Indirect	0.14–0.16	0.45–0.55	1.75–1.80	1.90–1.95	0.15
	+5%	1.55–1.60	Direct	0.14–0.16	0.40–0.50	1.80–1.85	1.95–2.00	0.15
$MoSe_2$	−5%	1.10–1.20	Indirect	0.18–0.22	0.40–0.50	1.55–1.65	1.75–1.85	0.20
	+5%	1.35–1.45	Direct	0.18–0.22	0.35–0.45	1.60–1.70	1.80–1.90	0.20

Table 3.2. provides a comprehensive summary of the strain-dependent electronic and excitonic properties of monolayer MoS_2 and $MoSe_2$, highlighting several important trends. First, the transition from indirect to direct band gap is clearly observed when the strain changes from compressive (−5%) to tensile (+5%) for both materials. This indicates that tensile strain stabilizes the direct band gap at the K point, which is crucial for enhancing optical absorption and emission efficiency. In contrast, compressive strain shifts the band extrema away from the K point, resulting in an indirect band gap and reduced radiative recombination efficiency. Second, the spin–orbit coupling-induced splitting (ΔSO) remains nearly constant under different strain conditions for each material, with values of approximately 0.14–0.16 eV for MoS_2 and 0.18–0.22 eV for $MoSe_2$. This suggests that SOC is primarily determined by the intrinsic atomic properties, particularly the heavier Se atom, rather than external lattice deformation. Third, the exciton binding energy (Eb) shows a slight decrease under tensile strain for both materials. This reduction can be attributed to increased lattice spacing, which weakens the Coulomb interaction between electrons and holes. As a result, excitons become less tightly bound under tensile conditions.

In addition, the A and B exciton energies exhibit systematic shifts with strain. Under tensile strain, both excitonic peaks shift toward lower energies (redshift), while compressive strain leads to higher-energy transitions (blueshift). Importantly, the energy separation between A and B excitons (ΔA–B) remains nearly constant for each material and closely matches the corresponding ΔSO values. This confirms that the excitonic splitting originates directly from the SOC-induced valence band splitting. Finally, a comparison between the two materials reveals that $MoSe_2$ exhibits stronger SOC effects, smaller band gap, and larger ΔA–B splitting, whereas MoS_2 shows higher exciton binding energy and sharper optical transitions. These differences highlight the complementary nature of the two materials and suggest that MoS_2 is more suitable for strong light–matter interaction applications, while $MoSe_2$ is advantageous for spintronic and valleytronic functionalities.

3.4. Combined Effects of Strain and Spin–Orbit Coupling

The evolution of the band structures under strain, including SOC, is shown in Figure 3.3.

Figure 3.3. Band structures under strain conditions with SOC

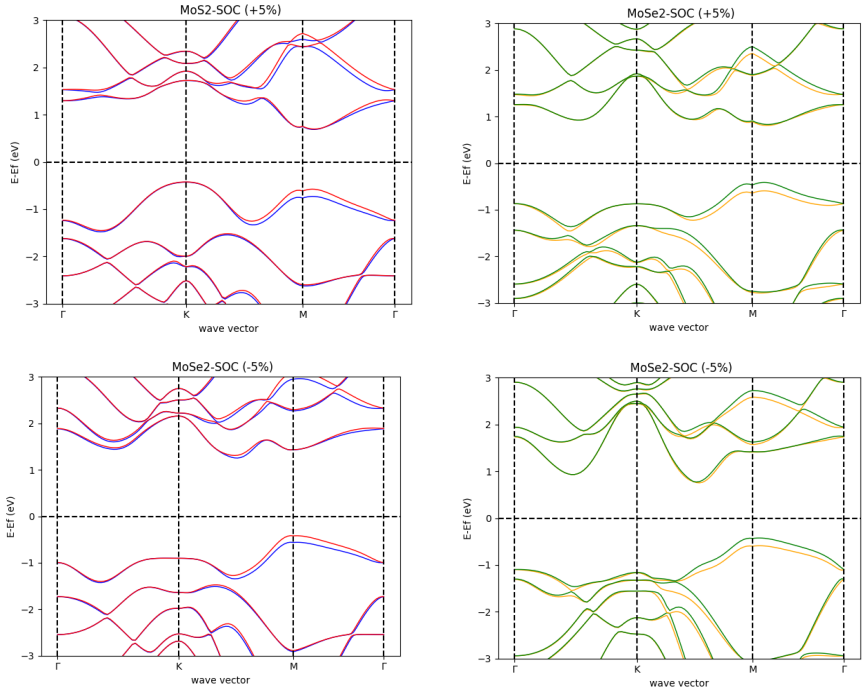

The results demonstrate that the SOC-induced splitting at the VBM persists under all strain conditions, confirming its robustness against structural deformation. However, strain significantly modifies the relative positions of the band extrema. Under tensile strain (+5%), both MoS_2 and $MoSe_2$ maintain their direct band gap at the K point, as clearly observed in the top panels of Figure 3.3, where both the VBM and CBM are located at K. In contrast, under compressive strain (−5%), a noticeable shift of the conduction band minimum (CBM) occurs away from the K point. Specifically, the CBM moves toward the so-called Q point, which is located along the Γ–K high-symmetry path (between Γ and K, approximately at ~2/3 of the Γ–K distance). In the band structures shown in Figure 3.3, this corresponds to the local minimum appearing between Γ and K, rather than exactly at either high-symmetry point.

As a result, the band gap transitions from direct (K–K) to indirect (K–Q or K–Γ), particularly evident in $MoSe_2$ under −5% strain, where the CBM at Q becomes lower in energy than that at K. This indirect transition reduces the probability of radiative recombination and thus weakens optical emission. Additionally, strain slightly modifies the magnitude of the VBM splitting, thereby influencing the energy separation between A and B excitons. These results highlight the strong interplay between lattice deformation and spin–orbit coupling, providing an effective mechanism for tuning both electronic and optical properties in two-dimensional TMDCs.

3.5. Optical Properties and Exciton Behavior

The optical properties of monolayer MoS_2 and $MoSe_2$ under different strain conditions are presented in Figure 3.4, including both the absorption spectra and the emission-related behavior inferred from the low-energy optical response.

Figure 3.4. Optical absorption and emission spectra under strain

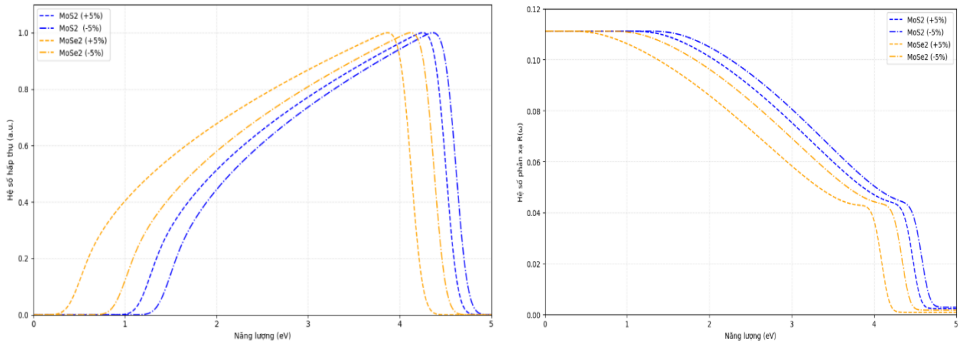

As shown in Figure 3.4, both materials exhibit strong optical absorption in the visible region, with a clear onset corresponding to their direct band gaps at the K point. The absorption edge of $MoSe_2$ appears at lower photon energies compared to MoS_2, indicating a pronounced redshift, which is consistent with its smaller band gap. This trend is clearly observed across all strain conditions. Under the influence of biaxial strain, the absorption spectra show a systematic shift:

- Tensile strain (+5%) shifts the absorption edge toward lower energies (redshift),
- Compressive strain (−5%) shifts it toward higher energies (blueshift).

This behavior is directly correlated with the strain-induced modulation of the band gap discussed in previous sections. Notably, $MoSe_2$ exhibits a more significant spectral shift compared to MoS_2, confirming its higher sensitivity to lattice deformation. In addition to absorption, the emission characteristics (photoluminescence-like behavior) can be inferred from the low-energy region of the spectra. The emission peaks, associated with radiative recombination of A excitons, follow the same trend as the absorption edge:

- A redshift in emission peaks under tensile strain,
- A blueshift under compressive strain.

This indicates that strain effectively tunes both excitation and recombination processes, making these materials highly adaptable for wavelength-selective optoelectronic applications. Furthermore, differences in spectral shape can be observed between the two materials. MoS_2 exhibits a sharper absorption edge and steeper spectral profile, which can be attributed to its larger exciton binding energy and stronger Coulomb interaction. In contrast, $MoSe_2$ shows a more gradual absorption onset and broader spectral features, reflecting enhanced dielectric screening and weaker exciton confinement. At higher photon energies, both materials display a rapid decrease in absorption intensity, indicating the transition beyond the dominant interband transitions. The strain-dependent shift of this region further confirms the strong coupling between electronic structure and optical response.

The distinct electronic and optical properties of MoS_2 and $MoSe_2$ suggest different application potentials. MoS_2, with its larger band gap and stronger exciton binding, is highly suitable for light-emitting devices and photodetectors. In contrast, $MoSe_2$, with its narrower band gap and stronger SOC, is promising for infrared optoelectronics and spintronic/valleytronic applications. Importantly, strain engineering combined with SOC effects provides a powerful strategy to tailor band structures and excitonic properties. This tunability opens new opportunities for designing next-generation nanoscale optoelectronic devices based on two-dimensional TMDC materials.

4. Conclusion

In this work, the electronic structure and optical properties of monolayer MoS_2 and $MoSe_2$ have been systematically studied using DFT calculations with inclusion of spin–orbit coupling. Both materials exhibit direct band gaps at the K point, with $MoSe_2$ showing a smaller band gap and stronger SOC-induced valence band splitting compared to MoS_2. This splitting leads to the formation of A and B excitons, whose energy separation is consistent with the magnitude of SOC. The application of biaxial strain demonstrates an effective approach to tune the band structure and optical response. Tensile strain reduces the band gap and induces a redshift in excitonic transitions, while compressive strain can lead to band gap widening and possible indirect transitions. $MoSe_2$ is found to be more sensitive to strain, making it a promising candidate for strain-engineered devices.

Furthermore, the optical analysis reveals strong excitonic effects in both materials, with MoS_2 exhibiting higher exciton binding energy and more pronounced optical peaks. In contrast, $MoSe_2$ benefits from stronger spin–orbit interaction, which is advantageous for spintronic and valleytronic applications. Overall, this study provides a comprehensive understanding of the interplay between strain and SOC in MoX_2 monolayers. The obtained results offer important guidelines for tailoring the electronic and optical properties of two-dimensional materials for applications in optoelectronics, photonics, and next-generation quantum devices.

Acknowledgements. This research was funded by Hoa Binh University foundation for Sciences and Technology Development via grant number: HB2025.ĐT.04.

References

[1] Q. H. Wang *et al.*, "Electronics and optoelectronics of two-dimensional transition metal dichalcogenides," *Nat. Nanotechnol.*, vol. 7, pp. 699–712, 2012.

[2] S. Manzeli *et al.*, "2D transition metal dichalcogenides," *Nat. Rev. Mater.*, vol. 2, 2017.

[3] K. F. Mak *et al.*, "Atomically thin MoS_2: A new direct-gap semiconductor," *Phys. Rev. Lett.*, vol. 105, no. 13, 2010.

[4] A. Splendiani *et al.*, "Emerging photoluminescence in monolayer MoS_2," *Nano Lett.*, vol. 10, no. 4, pp. 1271–1275, 2010.

[5] T. Cao *et al.*, "Valley-selective circular dichroism of monolayer MoS_2," *Nat. Commun.*, vol. 3, 2012.

[6] A. Chernikov *et al.*, "Exciton binding energy and nonhydrogenic Rydberg series in monolayer WS_2," *Phys. Rev. Lett.*, vol. 113, 2014.

[7] A. Ramasubramaniam, "Large excitonic effects in monolayer MoS_2," *Phys. Rev. B*, vol. 86, 2012.

[8] K. He *et al.*, "Tightly bound excitons in monolayer WSe_2," *Phys. Rev. Lett.*, vol. 113, 2014.

[9] D. Xiao *et al.*, "Coupled spin and valley physics in monolayers of MoS_2 and other TMDCs," *Phys. Rev. Lett.*, vol. 108, 2012.

[10] Z. Y. Zhu *et al.*, "Giant spin–orbit-induced spin splitting in monolayer TMDCs," *Phys. Rev. B*, vol. 84, 2011.

[11] A. Molina-Sánchez *et al.*, "Effect of spin–orbit interaction on the optical spectra of single-layer TMDCs," *Phys. Rev. B*, vol. 88, 2013.

[12] H. J. Conley *et al.*, "Bandgap engineering of strained monolayer and bilayer MoS_2," *Nano Lett.*, vol. 13, no. 8, pp. 3626–3630, 2013.

[13] J. Feng *et al.*, "Strain-engineered artificial atom as a broad-spectrum solar energy funnel," *Nat. Photonics*, vol. 6, 2012.

[14] H. Shi *et al.*, "Quasiparticle band structures and optical properties of strained monolayer MoS_2," *Phys. Rev. B*, vol. 87, 2013.

[15] S. Tongay *et al.*, "Broad-range modulation of light emission in TMDCs by strain," *Nano Lett.*, vol. 13, 2013.

[16] P. Hohenberg and W. Kohn, "Inhomogeneous electron gas," *Phys. Rev.*, vol. 136, 1964.

[17] W. Kohn and L. J. Sham, "Self-consistent equations including exchange and correlation effects," *Phys. Rev.*, vol. 140, 1965.

[18] G. Kresse and J. Furthmüller, "Efficient iterative schemes for *ab initio* total-energy calculations using a plane-wave basis set," *Phys. Rev. B*, vol. 54, 1996.

[19] G. Kresse and D. Joubert, "From ultrasoft pseudopotentials to the projector augmented-wave method," *Phys. Rev. B*, vol. 59, 1999.

[20] G. Kresse and J. Hafner, "Ab initio molecular dynamics for liquid metals," *Phys. Rev. B*, vol. 47, pp. 558–561, 1993.

[21] P. E. Blöchl, "Projector augmented-wave method," *Phys. Rev. B*, vol. 50, pp. 17953–17979, 1994.

[22] J. P. Perdew, K. Burke, and M. Ernzerhof, "Generalized gradient approximation made simple," *Phys. Rev. Lett.*, vol. 77, pp. 3865–3868, 1996.

[23] K. Lee *et al.*, "Higher-accuracy van der Waals density functional," *Phys. Rev. B*, vol. 82, 081101, 2010.

[24] J. Klimeš, D. R. Bowler, and A. Michaelides, "Van der Waals density functionals applied to solids," *Phys. Rev. B*, vol. 83, 195131, 2011.

[25] H. J. Monkhorst and J. D. Pack, "Special points for Brillouin-zone integrations," *Phys. Rev. B*, vol. 13, pp. 5188–5192, 1976.

[26] A. Kormányos *et al.*, "k·p theory for two-dimensional TMDC semiconductors," *2D Mater.*, vol. 2, 2015.

[27] H. Peelaers and C. G. Van de Walle, "Effects of strain on band structure of MoS_2," *Phys. Rev. B*, vol. 86, 241401, 2012.

[28] M. Gajdoš, K. Hummer, G. Kresse, J. Furthmüller, and F. Bechstedt, "Linear optical properties in the projector-augmented wave methodology," *Phys. Rev. B*, vol. 73, 045112, 2006.